



Universiteit  
Leiden  
The Netherlands

## Hydrogen dissociation on metal surfaces

Wijzenbroek, M.

### Citation

Wijzenbroek, M. (2016, June 2). *Hydrogen dissociation on metal surfaces*. Retrieved from <https://hdl.handle.net/1887/39935>

Version: Not Applicable (or Unknown)

License: [Licence agreement concerning inclusion of doctoral thesis in the Institutional Repository of the University of Leiden](#)

Downloaded from: <https://hdl.handle.net/1887/39935>

**Note:** To cite this publication please use the final published version (if applicable).

Cover Page



Universiteit Leiden



The handle <http://hdl.handle.net/1887/39935> holds various files of this Leiden University dissertation

**Author:** Wijzenbroek, Mark

**Title:** Hydrogen dissociation on metal surfaces

**Issue Date:** 2016-06-02

# CHAPTER 6

## Performance of a non-local van der Waals density functional on the dissociation of H<sub>2</sub> on metal surfaces

This chapter is based on:

M. WIJZENBROEK, D. M. KLEIN, B. SMITS, M. F. SOMERS, and G. J. KROES. Performance of a non-local van der Waals density functional on the dissociation of H<sub>2</sub> on metal surfaces. *Journal of Physical Chemistry A* **119**(50), pp. 12146–12158, 2015.

- 
- 6.1 Introduction 176
  - 6.2 Theory 181
    - Dynamical model 181 • Construction of potential energy surfaces 182 • Computational details 184
  - 6.3 Results and discussion 185
    - Potential energy surfaces and barrier heights 185 • Molecular beam sticking 191 • State-resolved reaction probability and rotational quadrupole alignment 192 • The effect of changing the exchange and the correlation functionals separately 197
  - 6.4 Conclusions and outlook 199
- References 201
-

## Abstract

Van der Waals functionals have been applied in chapter 4 to obtain a potential energy surface to describe the dissociation of  $\text{H}_2$  on  $\text{Ru}(0001)$ . An improvement was found for computed reaction probabilities compared to experiment, which could not be achieved with the use of other exchange–correlation functionals. It is, however, not yet clear to what extent van der Waals functionals give a better description of other molecule–metal surface systems. In this chapter, the optPBE-vdW-DF functional is compared to the SRP48 functional, which was originally fitted to describe the dissociation of  $\text{H}_2$  on  $\text{Cu}(111)$ , in terms of the resulting potential energy surfaces and results of quasi-classical dynamics calculations and their agreement with experiment for different  $\text{H}_2$ –metal surface systems. It is found that overall the optPBE-vdW-DF functional yields potential energy surfaces which are very similar to potential energy surfaces computed with the SRP48 functional. In dynamics calculations the optPBE-vdW-DF functional gives a slightly better description of molecular beam experiments. Also a different dependence of reaction on the rotational quantum number  $J$  is found, which is in better agreement with experimental data for  $\text{H}_2$  dissociation on  $\text{Cu}(111)$ . The vibrational efficacy is found to be relatively insensitive to which of the two functionals is chosen.

## 6.1 Introduction

To perform accurate calculations on molecule–surface reactions, it is important to have an accurate potential energy surface (PES). It is, however, not clear which precise electronic structure method should be used to compute such a PES in order to obtain a desirable accuracy. In practice, due to limitations in computational power, one is limited to density functional theory (DFT)<sup>1,2</sup> using approximate exchange–correlation (XC) functionals. These functionals are usually taken to be generalized gradient approximation (GGA)<sup>3–8</sup> level functionals due to the larger computational expense of higher level methods such as meta-generalized gradient approximation (meta-GGA)<sup>9–11</sup> level functionals, and hybrid functionals,<sup>12</sup> which introduce Hartree–Fock exchange into

the functional. Additionally, because for such systems often only dynamical properties such as reaction probabilities are known from experiments, and no or little knowledge is available from higher level electronic structure methods, it is often necessary to perform dynamics calculations<sup>13,14</sup> in order to benchmark electronic structure methods. This further makes such investigations computationally challenging, as either a high dimensional PES is needed, or dynamics needs to be performed based on energies and forces computed directly on the DFT level in *ab initio* molecular dynamics (AIMD) calculations.

One particular example of molecule–metal surface reactions is the dissociation of H<sub>2</sub> on metal surfaces. This particular example is a useful benchmark system for electronic structure methods, for several reasons. First of all, a large amount of experimental data is available for such systems. Additionally, these systems have also been well studied in theoretical calculations using various electronic structure and dynamics methods (see for instance references 13–23).

Second, in general molecule–surface systems are rather complex because, apart from the degrees of freedom of the molecule, in principle also degrees of freedom from the surface should be included, such as phonons and electron–hole pair excitations.<sup>15,24,25</sup> It is however expected for hydrogen dissociation on metal surfaces that the effects associated with these degrees of freedom are rather limited. For H<sub>2</sub> dissociation on metal surfaces the neglect of electron–hole pair excitations and surface motion seems to be a good approximation. It has been argued<sup>16</sup> for H<sub>2</sub> dissociation on Pt(111) that electron–hole pair excitations should not play an important role in such processes. Additionally, for H<sub>2</sub> dissociation on Cu(111),<sup>26,27</sup> Cu(110)<sup>28</sup> and Ru(0001)<sup>22</sup> non-adiabatic effects have been taken into account in dynamical calculations using electronic friction. In these calculations no large non-adiabatic effects were found, which suggests that for H<sub>2</sub>–metal systems the Born–Oppenheimer approximation works well. Furthermore, for activated dissociation systems energy exchange with phonons is expected to be a small effect<sup>29,30</sup> due to the large mass mismatch between the H<sub>2</sub> molecule and a metal surface atom. The validity of the neglect of surface motion and surface temperature has been recently tested for H<sub>2</sub> dissociation on Cu(111), using AIMD calculations,<sup>21</sup> in which the surface atoms were allowed to

move. Additionally, calculations have been performed in chapter 3 on the same system using a static corrugation model (SCM), in which energy exchange with the surface is not possible, but the displacement of surface atoms and thermal expansion of the crystal lattice are taken into account. In particular, in both studies, a good agreement with ideal static surface calculations was found for  $\text{H}_2$  dissociation on a low temperature Cu(111) surface ( $T_s = 120$  K).

Finally, because hydrogen is a small and simple molecule, if the surface degrees of freedom are neglected, the PES of the reaction is relatively simple (6-dimensional) and it becomes feasible to accurately map out the PES. Additionally, symmetry is often present in the systems of interest and thus can often be applied in the construction of the PES, as is often done in for example the corrugation reducing procedure (CRP).<sup>31,32</sup> The application of symmetry can often reduce the computational costs for PESs for  $\text{H}_2$  dissociation on ideal low-index surfaces considerably. Hydrogen–metal surface systems thus are useful for benchmarking the performance of electronic structure methods for molecule–surface reactions.<sup>25</sup>

It has been shown in chapter 4 for hydrogen dissociation on Ru(0001), which is a system with low barriers to reaction, that a functional containing vdW-DF<sup>33</sup> or vdW-DF2<sup>34</sup> correlation was needed to obtain a good agreement with experimental data, and that other functionals did not give a proper ‘width’ of the reaction probability as a function of incidence energy. It is however not yet clear to what extent vdW-DF-like functionals improve or worsen agreement for other systems, such as systems with a high barrier to reaction like  $\text{H}_2$  dissociation on Cu(111) or Cu(100), or other systems with low barriers to reaction such as  $\text{H}_2$  dissociation on Pt(111).

One of the problems of DFT for molecule–surface reactions is that computed barrier heights are often not in agreement with experiments and can differ wildly for different functionals, as shown in chapter 4 and reference 18. It is known that, for barriers of gas-phase reactions, using GGA level functionals mean absolute errors are obtained which are at best 4 kcal/mol.<sup>35–37</sup> Recently, fitted functionals on the meta-GGA level have been proposed claiming mean absolute errors of about 2 kcal/mol.<sup>37–40</sup> It is however not clear how such functionals would

perform for molecule–surface reactions as such systems have not been considered for the fitting set of these functionals.

To address the problem of accuracy in DFT, DÍAZ *et al.*<sup>18</sup> proposed an implementation of the specific reaction parameter (SRP) approach<sup>41</sup> in which the XC functional is adapted to the system at hand by optimising  $\alpha$  in

$$E_{\text{XC}}^{\text{SRP}} = \alpha E_{\text{XC}}^1 + (1 - \alpha) E_{\text{XC}}^2, \quad (6.1)$$

where  $E_{\text{XC}}^1$  and  $E_{\text{XC}}^2$  are two ‘standard’ (*i.e.*, GGA level) XC functionals, of which one generally tends to provide barriers which are too low, while the other generally provides barriers which are too high. Standard XC functionals used for molecule–surface reactions are the PW91<sup>6</sup> (or the similar PBE7) and RPBE<sup>8</sup> functionals. The optimisation of  $\alpha$  is done in such a way that an important experiment which provides information about the barrier height is well described. As a result, one hopes that the barrier heights for the system are well described and that other observables that have not been fitted are better described for the system considered. The downside of such a procedure however is that it gives only limited predictive power, as for each specific system of interest in principle at least one experiment is needed in order to construct such a functional, which then is specific to one particular system. The quality of the description thus relies on the quality of the experiment to which the functional was fitted. Note however that the functional which was fitted for H<sub>2</sub> dissociation on Cu(111)<sup>18</sup> could also give a reasonable description of experimental data of H<sub>2</sub> dissociation on Cu(100),<sup>42</sup> suggesting that an XC functional which works well for one system may also work well for a sufficiently similar system.

In the present study an SRP approach is not taken. Instead, in order to investigate to what extent current XC functionals can describe H<sub>2</sub>–metal surface systems, and to what extent van der Waals effects are needed for a description of such systems, the performance of functionals for not one but several H<sub>2</sub>–metal systems is considered. The H<sub>2</sub>/Cu(111), H<sub>2</sub>/Cu(100), H<sub>2</sub>/Pt(111) and H<sub>2</sub>/Ru(0001) systems are considered, because relatively well characterised experimental data is available for these systems. Two functionals are considered, one with a non-local van der Waals correction to the correlation functional and one

without. For the non-corrected functional SRP48<sup>21</sup> is taken, as this functional gives a good agreement with experiments for H<sub>2</sub>/Cu(111).

Over the past years, the inclusion of van der Waals effects in DFT has gathered a large interest, in particular for the interaction of molecules with surfaces.<sup>43–47</sup> Many methods to incorporate van der Waals effects in DFT have been developed, including the vdW-DF method by DION *et al.*,<sup>33</sup> the DFT-D3 method by GRIMME *et al.*<sup>48</sup> and the PBE+vdW method by TKATCHENKO and SCHEFFLER.<sup>49</sup> For a full overview, the reader is referred to recent review papers, such as references 44 or 45. In the vdW-DF method non-local correlation is used in an XC functional instead of standard (semi-)local correlation. Several revisions of this method have been published, including revisions of the vdW-DF correlation functional such as vdW-DF2,<sup>34</sup> but also functionals in which other exchange functionals such as optB88 and optPBE,<sup>50</sup> optB86b,<sup>51</sup> C09<sup>52</sup> and LV-PW86r,<sup>53</sup> are combined with the vdW-DF correlation functional. Recently, it has been shown for adsorption of benzene on transition metal surfaces that the optB88-vdW-DF and optPBE-vdW-DF functionals yield good adsorption energies, whereas the original vdW-DF and vdW-DF2 XC functionals yield adsorption energies that are smaller than the experimental values.<sup>54–56</sup> For H<sub>2</sub> dissociation on Ru(0001) it was found in chapter 4 that the vdW-DF and vdW-DF2 XC functionals yield barriers for reaction that are too high. For these reasons, here the optPBE-vdW-DF functional is chosen as the vdW-corrected functional to be tested. This functional has also recently been tested for the dissociation of N<sub>2</sub> on W(110).<sup>57</sup>

In section 6.2 the methods used are explained, beginning with the dynamical model in section 6.2.1. The construction of the PESs needed for the calculations is explained in section 6.2.2, and the computational details are given in section 6.2.3. The results are given in section 6.3, beginning with several properties and differences of the computed PESs in section 6.3.1. Molecular beam sticking results are shown in section 6.3.2 and state-resolved reaction probabilities and rotational quadrupole alignment parameters are considered in section 6.3.3. Effects of changing the exchange functional and correlation functional separately are discussed in section 6.3.4. Finally, the conclusions are given in section 6.4.

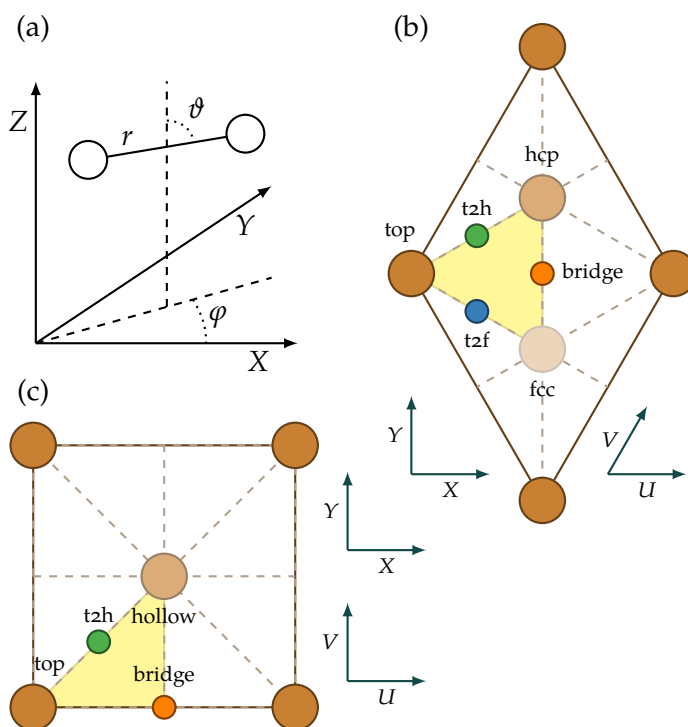


**FIGURE 6.1** (a) The center of mass coordinate system used for the description of the H<sub>2</sub> molecule. (b) The surface unit cell and the sites considered for the Cu(111), Pt(111) and Ru(0001) surfaces. (c) The surface unit cell and the sites considered for the Cu(100) surface. In both (b) and (c), the origin of the coordinate system ( $X = U = 0$ ,  $Y = V = 0$ ,  $Z = 0$ ) is at a top layer atom (top site). In (b), the fcc site is above a third layer atom for Cu(111) and Pt(111), but for Ru(0001) no surface atom is present at this site.

## 6.2 Theory

### 6.2.1 Dynamical model

In all calculations the Born–Oppenheimer static surface (BOSS) model is used. As suggested by the name of the model, first of all, the Born–Oppenheimer approximation<sup>58</sup> is used. Second, the surface atoms are taken to be fixed at their ideal lattice positions. As a result, only the 6 degrees of freedom of the H<sub>2</sub> molecule are taken into account in the dynamical model. In figure 6.1(a), the coordinate system used is shown,

in figure 6.1(b) the surface unit cell for the Cu(111), Pt(111) and Ru(0001) systems, and in figure 6.1(c) the surface unit cell for the Cu(100) system.

Quasi-classical dynamics calculations are performed in favour of quantum dynamics calculations for computational simplicity. For activated  $H_2$  and, in particular,  $D_2$  dissociation on metal surfaces, this is in general a good approximation, as shown for  $H_2$  dissociation on Cu(111),<sup>18,59,60</sup> Cu(100),<sup>61</sup> Ru(0001) (chapter 4) and Pt(111),<sup>62</sup> *i.e.*, for all systems considered here. In the dynamics calculations the Hamilton equations of motion are solved using the extrapolation method by STOER and BULIRSCH.<sup>63</sup> The initial conditions of the  $H_2$  molecules are selected using standard Monte Carlo methods. In order to obtain  $m_J$  resolved reaction probabilities, the initial angular momentum of the molecule is fixed by  $L = \sqrt{J(J+1)}\hbar$  and the orientation is chosen with the constraint  $\cos \vartheta_L = m_J / \sqrt{J(J+1)}$ , where  $\vartheta_L$  is the angle between the angular momentum vector and the surface normal. To obtain accurate statistics, for each set of incidence conditions at least  $10^4$  trajectories were computed. The  $H_2$  molecule is initially placed beyond the point where the PES no longer depends on  $Z$  ( $Z > 6.5 \text{ \AA}$ ). The molecule is considered to have dissociated when  $r > 2.25 \text{ \AA}$ , and the molecule is considered to have scattered when  $Z > 6.5 \text{ \AA}$  with the momentum vector pointing away from the surface.

### 6.2.2 Construction of potential energy surfaces

Full 6D PESs were constructed from self-consistent DFT calculations using the optPBE-vdW-DF<sup>50</sup> and SRP48<sup>21</sup> functionals. The SRP48 functional contains a linear combination of 48 % RPBE exchange<sup>8</sup> and 52 % PBE exchange<sup>7</sup> together with PBE correlation.<sup>7</sup> The optPBE-vdW-DF functional combines an optimized PBE-like exchange functional (optPBE<sup>50</sup>) with vdW-DF correlation.<sup>33</sup>

In the interpolation of the PESs the CRP,<sup>31,32</sup> discussed in section 2.1.1, is used. The idea behind the CRP is to interpolate  $I^{6D}$  instead of  $V^{6D}$ , as  $I^{6D}$  is much less corrugated in the  $U$ ,  $V$ ,  $\vartheta$  and  $\varphi$  degrees of freedom than  $V^{6D}$  is (see section 2.1.1 for the definition of these symbols).<sup>31</sup> The  $(U, V)$  coordinate system is a coordinate system in which the surface lattice vectors are taken as unit vectors. For  $H_2$  dissociation

**TABLE 6.1** Configurations used in the interpolation of the  $\text{H}_2/\text{Cu}(100)$  PESs. The sites listed here correspond to the sites listed in table 6.2, and are also shown graphically in figure 6.1(c).

Site	$\vartheta$ (°)	$\varphi$ (°)
Top	0	
Top	90	0, 45
t2h	0	
t2h	45	45, 135, 225
t2h	90	45, 135
Hollow	0	
Hollow	90	0, 45
Bridge	0	
Bridge	90	0, 45, 90

on  $\text{Cu}(111)$ ,  $\text{Pt}(111)$  and  $\text{Ru}(0001)$  the skewing angle of this coordinate system thus is  $60^\circ$ , while for  $\text{H}_2$  dissociation on  $\text{Cu}(100)$  the skewing angle is  $90^\circ$  as for the Cartesian coordinate system (also see figure 6.1(b) and (c)). The interpolation over  $U$ ,  $V$ ,  $\vartheta$  and  $\varphi$  is done using symmetry adapted functions, in a way similar to the method used for  $\text{H}_2/\text{Cu}(100)$  by OLSEN *et al.*<sup>32</sup> The interpolation procedure used for potentials for the  $\text{H}_2/\text{Cu}(111)$ ,  $\text{Pt}(111)$  and  $\text{Ru}(0001)$  systems is the same as used in chapter 4 for  $\text{H}_2/\text{Ru}(0001)$  ( $p3m1$  symmetry). The interpolation for  $\text{H}_2/\text{Cu}(100)$  ( $p4mm$  symmetry) is detailed below.

For the interpolation of  $I^{6D}$  for potentials with  $p4mm$  symmetry, 16 configurations ( $U$ ,  $V$ ,  $\vartheta$ ,  $\varphi$ ) are used, spread over 4 different sites ( $U$ ,  $V$ ). These sites are also shown in figure 6.1(c). The configurations used are shown in table 6.1. The interpolation is done in several steps. First, for every configuration, the interpolation is performed over the  $r$  and  $Z$  degrees of freedom. For this interpolation a  $14 \times 14$  ( $r \times Z$ ) grid is used employing a 2D cubic spline interpolation, where  $r_{\min} = 0.4 \text{ \AA}$ ,  $r_{\max} = 2.3 \text{ \AA}$ ,  $Z_{\min} = 0.25 \text{ \AA}$  and  $Z_{\max} = 4 \text{ \AA}$ . Then, for every site ( $U$ ,  $V$ ) the interpolation is performed over the  $\vartheta$  and  $\varphi$  degrees of freedom using symmetry adapted sine and cosine functions. Finally, an interpolation over  $U$  and  $V$  is performed, for which again symmetry adapted sine and

TABLE 6.2 Sites used in the interpolation of the H/Cu(100) PES.

Site	$u$	$v$
Top	0	0
t2h	1/4	1/4
Hollow	1/2	1/2
b2h	1/2	1/4
Bridge	1/2	0
t2b	1/4	0

cosine functions are used.

In order to represent interactions that are rather long-ranged in the potential, the potential is switched between  $Z = 3.4 \text{ \AA}$  and  $4.0 \text{ \AA}$  from the full 6D potential to a 2D gas-phase potential only dependent on  $r$  and  $Z$ , because far away from the surface the corrugation is small. This gas phase potential is represented by

$$V^{2D}(r, Z) = V^{\text{ext}}(Z) + V^{\text{gas}}(r), \quad (6.2)$$

where  $V^{\text{ext}}$  is a function describing the dependence of the PES on  $Z$  beyond  $Z = 4 \text{ \AA}$  and  $V^{\text{gas}}$  is the interaction at  $Z = Z_{\text{asy}}$ , taken to be  $6.5 \text{ \AA}$ .

For the interpolation of  $I^{3D}$  six sites in  $(u, v)$  are used for the potentials with p4mm symmetry, which are listed in table 6.2. The sites b2h and t2b correspond to the sites in between bridge and hollow, and top and bridge, respectively. For each site, 57 points are taken in  $Z$ , with  $Z_{\text{min}} = -1.06 \text{ \AA}$  and  $Z_{\text{max}} = 5.6 \text{ \AA}$ . The reference function  $V^{1D}$  is taken to be the H atom–surface interaction for the H atom above the top site, as used in previous studies.<sup>31</sup>

### 6.2.3 Computational details

For the electronic structure calculations version 5.2.12 of the VASP<sup>64–67</sup> software package was used. For calculations with the SRP48 functional, the standard<sup>68</sup> VASP ultrasoft pseudopotentials<sup>69</sup> were used. For the optPBE-vdW-DF functional, the standard<sup>67</sup> projector augmented wave

(PAW)<sup>70</sup> potentials were used. VASP evaluates the non-local vdW-DF correlation functional within the scheme of ROMÁN-PÉREZ and SOLER.<sup>71</sup>

For the computation of the PESs, a  $9 \times 9 \times 1$   $\Gamma$ -centered  $k$ -point mesh was used with a plane wave cut-off of 400 eV, except for the  $\text{H}_2/\text{Ru}(0001)$  PESs where a  $8 \times 8 \times 1$  mesh was used with a plane wave cut-off of 350 eV. For  $\text{H}_2$  dissociation on  $\text{Cu}(100)$  and  $\text{Cu}(111)$ , a 4 layer slab was used, while for  $\text{H}_2$  dissociation on  $\text{Ru}(0001)$  and  $\text{Pt}(111)$  a 5 layer slab was used, which is consistent with previous calculations<sup>16,18,42</sup> on these systems (see also chapter 4). In all cases a  $2 \times 2$  supercell was considered with a 13 Å vacuum between different images of the slab. Fermi smearing with a width of 0.1 eV was used to speed up convergence of the DFT calculations. The convergence with respect to the plane wave cut-off and  $k$ -point sampling was tested for  $\text{H}_2/\text{Cu}(111)$  and  $\text{H}_2/\text{Pt}(111)$  at three different geometries close to or at the barrier geometry and is expected to be well within 10 meV of the fully converged value.

## 6.3 Results and discussion

### 6.3.1 Potential energy surfaces and barrier heights

In table 6.3 barrier heights are given for three high symmetry dissociation paths for the computed PESs, together with the distance of the  $\text{H}_2$  molecule to the surface ( $Z$ ) and the distance between the two H atoms ( $r$ ) at the transition state. For the  $\text{H}_2/\text{Cu}(111)$  and  $\text{H}_2/\text{Cu}(100)$  systems, both functionals predict the lowest barrier to be for bridge-to-hollow (BtH) dissociation, consistent with previous calculations.<sup>18,42</sup> For these systems the energetic corrugation (denoted in table 6.3 by  $\xi$ , here defined as the difference between the highest and lowest investigated barrier) is smaller for the optPBE-vdW-DF functional than for the SRP48 functional. For the  $\text{H}_2/\text{Ru}(0001)$  and  $\text{H}_2/\text{Pt}(111)$  systems, both functionals predict the lowest barrier to be for top-to-bridge (TtB) dissociation, which is also consistent with previous calculations<sup>16,20,72</sup> (see also chapter 4). For these systems the optPBE-vdW-DF functional yields a larger energetic corrugation than the SRP48 functional. Compared to the SRP48 barrier heights, for the  $\text{H}_2/\text{Cu}(111)$  and  $\text{H}_2/\text{Cu}(100)$  systems the optPBE-vdW-DF functional generally predicts larger barrier heights,

**TABLE 6.3** Barrier heights ( $E_b$ ), positions ( $r_b$ ,  $Z_b$ ) and energetic corrugation ( $\zeta$ , in eV) for SRP48 and optPBE-vdW-DF PESs for  $H_2$  dissociation on Cu(111), Cu(100), Ru(0001) and Pt(111) above three different sites. For all geometries,  $\vartheta = 90^\circ$ . On the HCP and hollow sites,  $\varphi = 0^\circ$ . Also see figure 6.1(b) and figure 6.1(c) and the definitions given in the text.

		SRP48			optPBE-vdW-DF		
		$E_b$ (eV)	$r_b$ (Å)	$Z_b$ (Å)	$E_b$ (eV)	$r_b$ (Å)	$Z_b$ (Å)
<b>Cu(111)</b>	BtH	0.636	1.030	1.172	0.712	1.053	1.165
	TtB	0.887	1.396	1.394	0.915	1.382	1.396
	HCP	1.047	1.539	1.269	1.070	1.427	1.271
	$\zeta$	0.411			0.358		
<b>Cu(100)</b>	BtH	0.742	1.239	0.992	0.822	1.237	0.996
	HOL	0.836	1.099	1.031	0.896	1.112	1.050
	TtB	0.867	1.432	1.379	0.883	1.413	1.383
	$\zeta$	0.125			0.074		
<b>Ru(0001)</b>	TtB	0.066	0.757	2.650	-0.013	0.755	2.662
	BtH	0.281	0.789	1.997	0.219	0.793	1.934
	HCP	0.398	0.812	1.869	0.361	0.835	1.762
	$\zeta$	0.332			0.374		
<b>Pt(111)</b>	TtB	0.102	0.767	2.292	0.034	0.774	2.152
	HCP	0.490	0.847	1.669	0.506	0.874	1.602
	BtH	0.492	0.837	1.602	0.530	0.862	1.506
	$\zeta$	0.390			0.496		

whereas the optPBE-vdW-DF barrier heights for  $H_2$ /Ru(0001) are generally smaller. For  $H_2$ /Pt(111), the optPBE-vdW-DF barrier height is smaller for TtB dissociation, but larger for HCP and BtH dissociation.

The barrier positions for the two PESs are similar for the  $H_2$ /Cu(111) and  $H_2$ /Cu(100) systems, but are less similar for the  $H_2$ /Ru(0001) and  $H_2$ /Pt(111) systems, where the barriers for optPBE-vdW-DF are mostly closer to the surface than for SRP48. For  $H_2$ /Ru(0001), in chapter 4, where a large number of functionals were considered, it was found for the TtB barrier that functionals containing vdW-DF correlation predict a barrier closer to the surface than functionals containing another type of correlation, *e.g.*, PBE correlation as used in the SRP48 functional, for

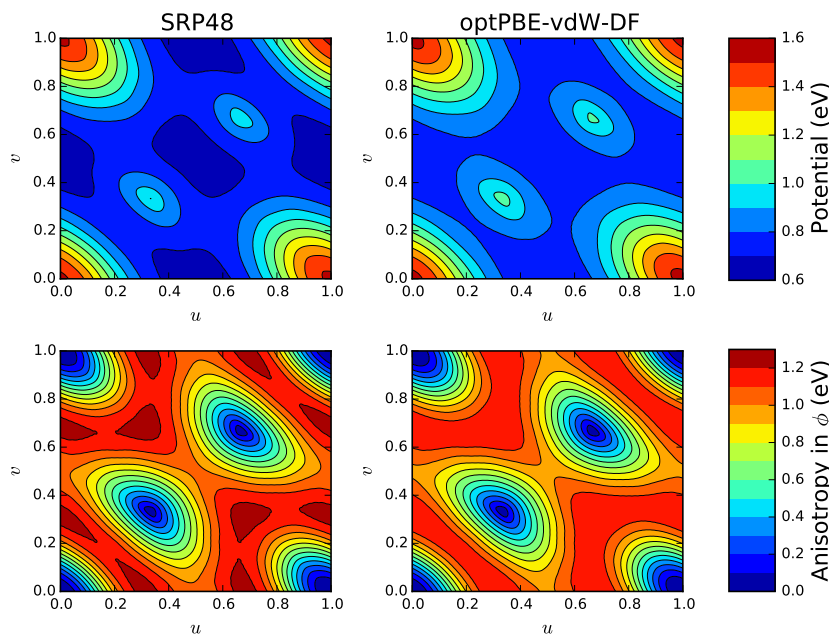


**FIGURE 6.2**  $(U, V)$  dependence of the PESs for  $\text{H}_2$  dissociation on  $\text{Cu}(111)$ , for  $r = 1.2 \text{ \AA}$ ,  $Z = 1.2 \text{ \AA}$  and  $\vartheta = 90^\circ$ . Top panels: full potential with  $\varphi$  optimized. Bottom panels: anisotropy in  $\varphi$ , as explained in the text.

a similar barrier height. The present results for  $\text{Ru}(0001)$ , but also for  $\text{Pt}(111)$ , are in agreement with this.

In figure 6.2 the  $(U, V)$  dependence of the SRP48 and optPBE-vdW-DF PESs for  $\text{H}_2$  dissociation on  $\text{Cu}(111)$  is shown, together with the anisotropy in  $\varphi$  at the same points, for a point ( $r = 1.2 \text{ \AA}$ ,  $Z = 1.2 \text{ \AA}$ ) close to the barrier geometry with  $\vartheta = 90^\circ$ . The anisotropy in  $\varphi$  is here defined as the difference between the highest and lowest potential encountered while rotating the molecule around  $360^\circ$  over  $\varphi$  for  $\vartheta = 90^\circ$ . The potential energy shown in the top panels is the minimum potential energy encountered during this rotation over  $\varphi$ .

The anisotropy of the two potentials close to the barrier geometry is remarkably similar, with the anisotropy for optPBE-vdW-DF being slightly lower than the anisotropy for SRP48. The remarkable similarity

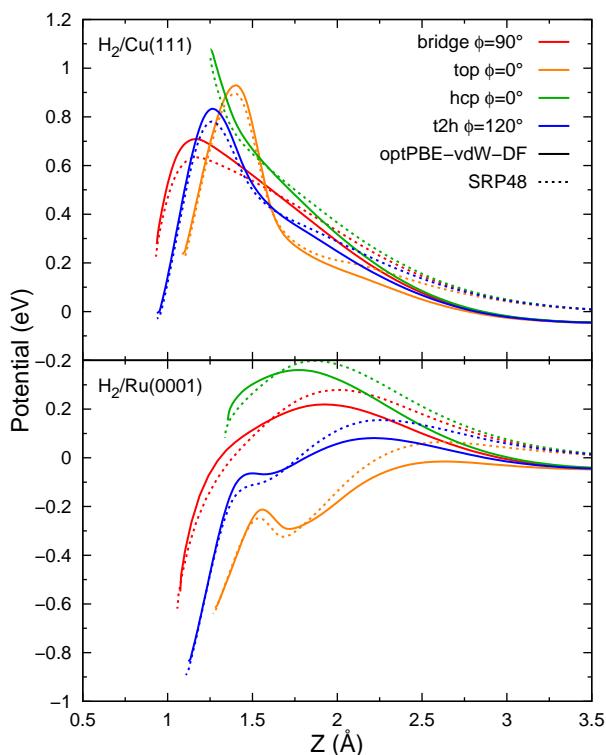


**FIGURE 6.3** Reaction paths based on nudged elastic band (NEB) calculations on a spline interpolation of computed 2D PES cuts for the  $\text{H}_2/\text{Cu}(111)$  and  $\text{H}_2/\text{Ru}(0001)$  systems, for four different dissociation geometries. A potential of 0 eV corresponds to the gas-phase minimum. Results for optPBE-vdW-DF are indicated by solid lines, while results for SRP48 are indicated by dotted lines.

between the SRP48 and optPBE-vdW-DF PESs for both the full potential, minimized over  $\varphi$ , and the anisotropy in  $\varphi$ , as well as the barrier positions shown in table 6.3, suggests that also dynamical observables that are dependent on more detailed properties of the PES, such as the anisotropy or the corrugation of the PES should be reasonably similar, except for a small shift or broadening due to the different barrier heights. Similar plots for the other systems considered show similar behaviour in the sense that the anisotropy of the SRP48 and optPBE-vdW-DF PESs is at least qualitatively similar.

Minimum energy paths were computed with the nudged elastic band (NEB) method applied to 2D cuts through the interpolated PES for  $H_2$  dissociation on Cu(111) and Ru(0001) for four different dissociation pathways. These pathways are shown in figure 6.3. Several features of the PES are apparent in this figure. First of all, far away from the surface, near  $Z = 3.5 \text{ \AA}$ , the optPBE-vdW-DF potential is lower than the SRP48 potential. This is a result of the van der Waals attraction, which leads to a well in the PES. This well is present in the optPBE-vdW-DF PESs, but not in the SRP48 PESs, as (semi-)local functionals such as SRP48 cannot describe van der Waals effects.<sup>45</sup> Beyond this well, moving the molecule closer to the surface, the PES for both functionals qualitatively changes in the same way: the ordering of the potential for different reaction paths is the same for both surfaces.

There are, however, some more subtle differences which seem to be relevant. First of all, for  $H_2$  dissociation on Cu(111), the optPBE-vdW-DF potential rises more quickly when the molecule is moved toward the surface than for the SRP48 potential. This causes the optPBE-vdW-DF and SRP48 potentials to cross one another at about  $Z = 1.6 \text{ \AA}$ . Second, for  $H_2$  dissociation on Ru(0001), similar effects occur although the effects seem smaller for this system. In this case a similar crossing occurs as for Cu(111), but here the crossing occurs after the SRP48 transition state, at about  $Z = 1.6 - 1.8 \text{ \AA}$ , similar to the crossing for Cu(111). In the optPBE-vdW-DF PES, the  $Z$  dependence of the potential for  $H_2$ /Ru(0001) is also somewhat stronger than in the SRP48 PES, although this effect seems to be smaller than for  $H_2$  dissociation on Cu(111). The barriers for  $H_2$  dissociation on Ru(0001) are generally closer to the surface for optPBE-vdW-DF than for SRP48.  $H_2$ /Cu(100) behaves similarly to  $H_2$ /Cu(111), while  $H_2$ /Pt(111) behaves similarly to  $H_2$ /Ru(0001).

It is clear that such effects should be present if a functional with a van der Waals correction is used which, additionally, gives the same or nearly the same description of the barrier height as the non-vdW functional, as is the case here. The interaction present in the regular, non-vdW corrected functional approximately starts at a value of  $Z$  which corresponds to the bottom of the van der Waals well. In order to obtain the same barrier height and position with the vdW functional that the

non-vdW functional would yield (the effective barrier from this point to reaction has gone up by the well depth), this non-vdW interaction in the vdW corrected functional either has to start earlier (at a larger value of  $Z$ ) or has to be stronger (*i.e.*, yields a stronger  $Z$  dependence of the potential). As shown in figure 6.3, the non-vdW interaction does not seem to start earlier for optPBE-vdW-DF than for SRP48 (an extrapolation of the SRP48 curves to the bottom of the well in figure 6.3 suggests the interaction should then start at  $Z \approx 3.5 \text{ \AA}$ ). As this is not the case, the  $Z$  dependence of the potential should be stronger. A proper van der Waals corrected functional for such systems is therefore expected to yield a steeper  $Z$  dependence than a non-vdW corrected functional would.

By considering these effects for early and late barriers it is possible to explain the differences between SRP48 and optPBE-vdW-DF barriers in table 6.3, as well as make more general predictions for differences between van der Waals and standard GGA functionals. Due to the steeper  $Z$  dependence of the PES, for late barriers, which occur beyond the crossing point ( $Z < 1.6 \text{ \AA}$ ), the barrier will in general be increased by going from SRP48 to optPBE-vdW-DF. For systems containing only late barriers, such as the highly activated  $\text{H}_2/\text{Cu}(111)$  and  $\text{H}_2/\text{Cu}(100)$  here, all barrier heights will therefore in general increase. For early barriers, which occur before the crossing point ( $Z > 1.8 \text{ \AA}$ ), the barrier will in general be decreased and occur at a smaller value of  $Z$  for the optPBE-vdW-DF functional. The results in table 6.3 are mostly in agreement with this. It should be noted that for  $\text{H}_2$  dissociation on  $\text{Ru}(0001)$  it was previously found that there is a trend between the barrier height and position, in the sense that higher barriers generally occur closer to the surface,<sup>72</sup> which was also found in chapter 4. For systems containing early barriers such as  $\text{H}_2/\text{Pt}(111)$  and  $\text{H}_2/\text{Ru}(0001)$  however, in general both earlier and later barriers will be present, and for these systems the later barrier heights therefore increase slightly compared to the earlier barrier heights, yielding an increased energetic corrugation. It should be noted that, in principle, these arguments can be extended to other pairs of well performing functionals and systems as well, provided that one knows where the crossing point for the two functionals occurs, which is determined by the steepness of the potential in  $Z$  and the depth of the

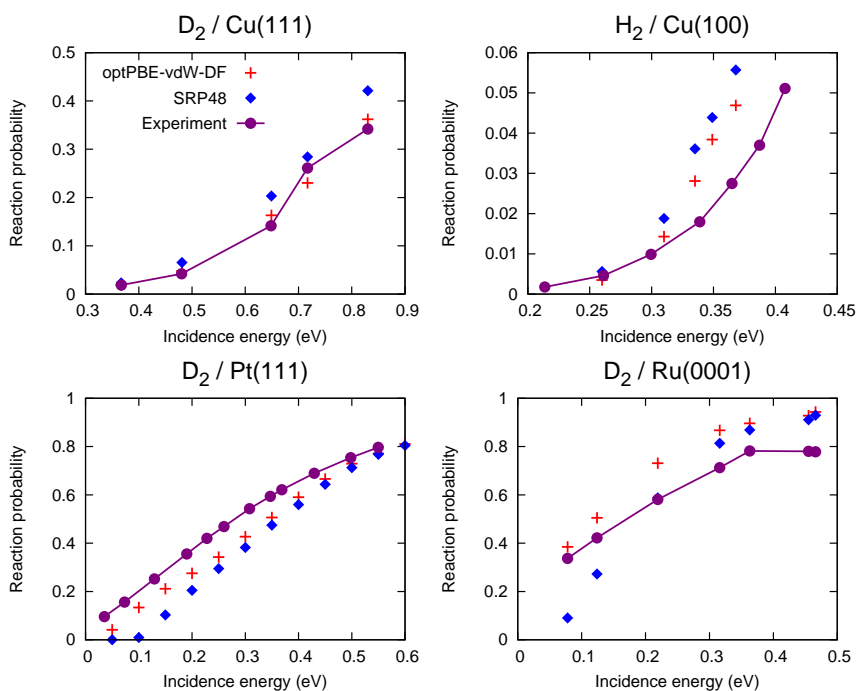


**FIGURE 6.4** Molecular beam simulations for the optPBE-vdW-DF and SRP48 functionals, applied to the four systems considered in this study. Beam parameters used for the Cu(111) and Cu(100) calculations were taken from DÍAZ *et al.*<sup>18</sup> Beam parameters used for the Ru(0001) calculations were taken from chapter 4. For the Pt(111) surface the ( $\nu = 0, J = 0$ ) reaction probability is shown as no beam parameters are known. Experimental data for Cu(111) by MICHELSEN *et al.*,<sup>73</sup> for Cu(100) by ANGER *et al.*,<sup>74</sup> for Pt(111) by LUNTZ *et al.*<sup>75</sup> and Ru(0001) by GROOT *et al.*<sup>76</sup>

physisorption well.

### 6.3.2 Molecular beam sticking

In figure 6.4 sticking probabilities are shown for  $D_2$  dissociation on Cu(111),  $H_2$  dissociation on Cu(100) and  $D_2$  dissociation on Ru(0001), and the initial state-resolved reaction probability is shown for ( $\nu = 0, J = 0$ )  $D_2$  dissociation on Pt(111), for the optPBE-vdW-DF and SRP48 functionals. A comparison is made with available experimental data.<sup>73–76</sup> As expected, for  $D_2$  dissociation on Cu(111) the SRP48 re-

action probability is in good agreement with experiment. This is not surprising because this functional was constructed<sup>18,21</sup> to reproduce this particular molecular beam experiment. The optPBE-vdW-DF functional also performs well, giving somewhat lower reaction probabilities in line with the higher barriers present in the PES (see table 6.3). For H<sub>2</sub> dissociation on Cu(100) the same holds. The agreement for the SRP48 functional is similar to that found in previous calculations with a similar functional,<sup>42</sup> and the agreement for the optPBE-vdW-DF functional is again somewhat better due to the higher barriers to dissociation given by this functional. For D<sub>2</sub> dissociation on Pt(111) and Ru(0001), however, the optPBE-vdW-DF functional gives higher reaction probabilities than the SRP48 functional. For D<sub>2</sub> dissociation on Pt(111), the agreement is better for the optPBE-vdW-DF functional than for the SRP48 functional. The optPBE-vdW-DF reaction probability rises less steeply with increasing incidence energy than the SRP48 reaction probability. Such a ‘broadening’ effect resulting from the use of XC functionals containing vdW-DF correlation was also found for hydrogen dissociation on Ru(0001) in chapter 4. Finally, for D<sub>2</sub> dissociation on Ru(0001), the SRP48 functional gives a reaction probability curve which is too narrow, which was also found in previous calculations with a similar functional.<sup>20</sup> The optPBE-vdW-DF functional gives a somewhat better width for the reaction probability curve and better agreement with experiment. Overall, for the systems considered here, the optPBE-vdW-DF functional tends to outperform the SRP48 functional.

### 6.3.3 State-resolved reaction probability and rotational quadrupole alignment

In figure 6.5 the reaction probability for ( $\nu = 0, J = 0$ ) and ( $\nu = 1, J = 0$ ) D<sub>2</sub> dissociating on Cu(111) is shown for the SRP48 and optPBE-vdW-DF functionals. Despite the difference in energetic corrugation (for SRP48  $\zeta = 0.411$  eV, while for optPBE-vdW-DF  $\zeta = 0.358$  eV), for neither ( $\nu = 0, J = 0$ ) nor ( $\nu = 1, J = 0$ ) D<sub>2</sub> noticeable differences are found between the slopes of the reaction probability curves obtained with the two functionals, which contrasts with the large difference found for H<sub>2</sub>

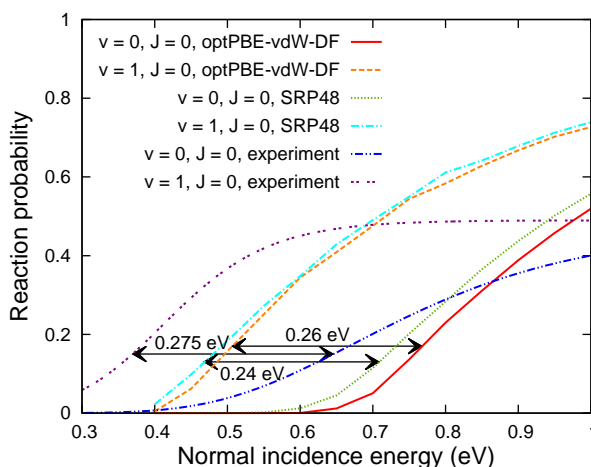


**FIGURE 6.5** Reaction probability as a function of normal incidence energy for ( $\nu = 0, J = 0$ )  $D_2$  and ( $\nu = 1, J = 0$ )  $D_2$  dissociating on Cu(111) for the SRP48 and optPBE-vdW-DF functionals.  $\Delta E_0$  at a reaction probability of 15% are indicated. Experimental data for  $T_s = 925$  K by MICHELSEN *et al.*,<sup>73</sup> reanalysed by NATTINO *et al.*<sup>77</sup>

**TABLE 6.4** Vibrational efficacy for ( $\nu = 0 \rightarrow 1$ )  $D_2$  dissociating on Cu(111).

Method	Vibrational efficacy
SRP48	0.65
optPBE-vdW-DF	0.71
Re-analysis <sup>77</sup> ( $P_{r,0} = 0.05$ )	0.62
Re-analysis <sup>77</sup> ( $P_{r,0} = 0.15$ )	0.74
Re-analysis <sup>77</sup> ( $P_{r,0} = 0.25$ )	0.88

dissociation on Ru(0001) in chapter 4. The ( $\nu = 0$ ) and ( $\nu = 1$ ) curves have a similar shape and slope for each functional, in disagreement with the results of the analysis of experiments, which show large differences between the slopes of ( $\nu = 0$ ) and ( $\nu = 1$ ) curves.<sup>73,77</sup> Note, however, that the effect of surface temperature is not taken into account in the calculations reported here, and it is known from experiments that this should cause a broadening of the reaction probability curves, which should be prominent at the experimental  $T_s$  (925 K).<sup>78,79</sup>

The use of the optPBE-vdW-DF functional leads to a slightly higher value of the vibrational efficacy ( $\chi_\nu = 0.71$ ) than the use of the SRP48 functional ( $\chi_\nu = 0.65$ ) (see table 6.4). This reflects the slightly larger shift of the ( $\nu = 1$ ) reaction probability curve relative to the ( $\nu = 0$ ) curve for the optPBE-vdW-DF functional (0.26 eV) than observed for the SRP48 functional (0.24 eV, see equation (2.40)). These numbers can be compared to the value of  $\chi_\nu$  that can be obtained from a recent re-analysis<sup>77</sup> of the original experimental data.<sup>73</sup> This experimental value depends on the value selected for  $P_{r,0}$  used to define  $E_0$  in equation (2.40) (see section 2.5.4) because the shapes of the reaction probability curves for ( $\nu = 1$ ) and ( $\nu = 0$ ) extracted from experiment differ: for  $P_{r,0} = 0.15$ ,  $\chi_\nu = 0.74$  is obtained, and for  $P_{r,0} = 0.05$ ,  $\chi_\nu = 0.62$  (see table 6.4). To which theoretical value of  $\chi_\nu$  the experimental value should be compared is not so straightforward. The experimental fits could be argued to be the most accurate where the time-of-flight (TOF) intensity is highest. For ( $\nu = 0, J = 0$ ) this is at a reaction probability of about 0.1. On the other hand, the reaction probability at the so-called effective barrier height in the old experimental fits was 0.135 and 0.25, for  $\nu = 0$  and  $\nu = 1$ , respectively. To a good approximation, at the corresponding collision energy the reaction probability does not vary with  $T_s$ .<sup>78,79</sup> A useful compromise therefore seems to be to evaluate the vibrational efficacy for a reaction probability of about 0.15. As it is not fully clear which reaction probability should be considered, the vibrational efficacy is shown for several values of the reaction probability in table 6.4. On the basis of these values, no preference for SRP48 or optPBE-vdW-DF can be found from the calculated  $\chi_\nu$ , as both functionals perform equally well. Finally, note that the experimental value for  $D_2/\text{Cu}(111)$  was originally reported to be  $\chi_\nu = 0.54$ ,<sup>73</sup> but this was based on a different definition of the vibrational efficacy, in which different values for  $P_{r,0}$  are used for  $\nu = 0$  and  $\nu = 1$ .

In figure 6.6 the reaction probability for ( $\nu = 0, J = 0, 2, 4, 6, 8$ )  $D_2$  dissociating on  $\text{Cu}(111)$  is shown for both tested functionals, also comparing to the reaction probability curves extracted from experiments.<sup>77</sup> The analysis of the experimental results showed that reaction first decreases with  $J$ , up to about  $J = 4$ , and then increases with  $J$ .<sup>73,77</sup> The behaviour of the optPBE-vdW-DF results is closest to this: for optPBE-

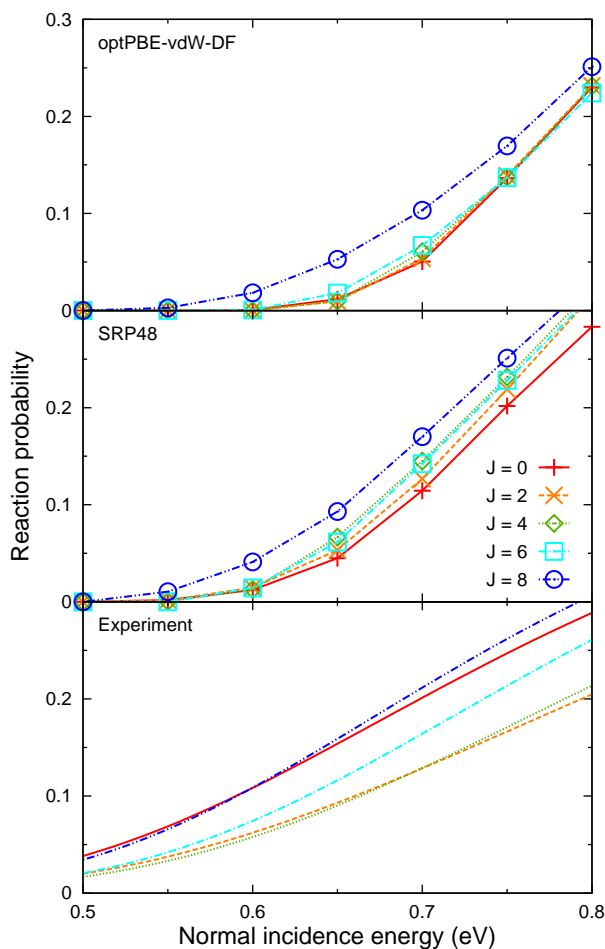


**FIGURE 6.6** Reaction probability as a function of normal incidence energy for several rotational states of  $D_2$  dissociating on Cu(111) for the optPBE-vdW-DF and SRP48 functionals. Fits to experimental results<sup>73</sup> at  $T_s = 925$  K by NATTINO *et al.*<sup>77</sup>

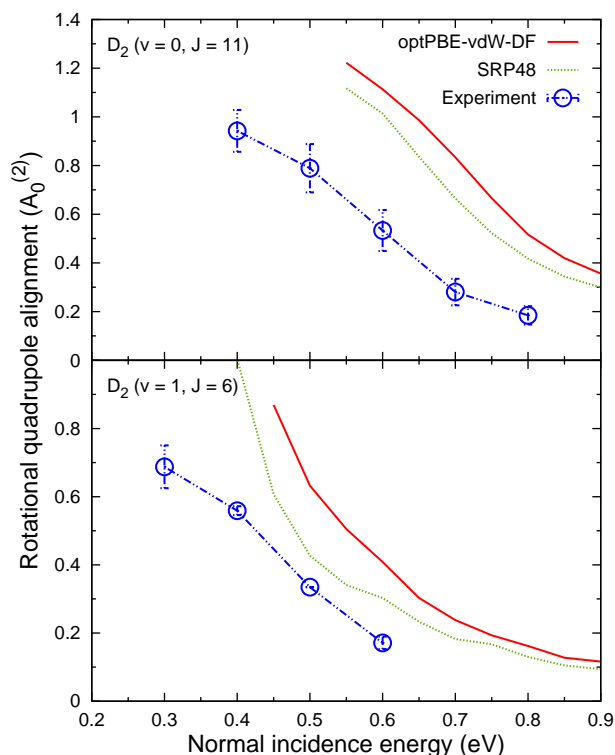


**FIGURE 6.7** Rotational quadrupole alignment parameter for  $D_2$  dissociation on Cu(111) as a function of normal incidence energy for the optPBE-vdW-DF and SRP48 functionals. Experimental results at  $T_s = 925$  K by Hou *et al.*<sup>80</sup>

vdW-DF, up to  $J = 6$  no large dependence of reaction on  $J$  is found, and for higher  $J$  the reaction probability increases with  $J$ . For the SRP48 functional, however, reaction actually increases up to about  $J = 4$ , in direct contrast to the behaviour observed in experiment. The optPBE-vdW-DF functional therefore seems to show a somewhat better performance than the SRP48 functional.

The rotational quadrupole alignment parameter  $A_0^{(2)}(\nu, J)$  is shown in figure 6.7 for  $(\nu = 0, J = 11)$  and  $(\nu = 1, J = 6)$   $D_2$  dissociating on Cu(111) for both functionals, also comparing to experiments.<sup>80</sup> The  $A_0^{(2)}(\nu, J)$  computed with SRP48 is shifted to lower energies than the one computed with optPBE-vdW-DF for both states at all energies considered, by about 0.05 eV for  $(\nu = 0, J = 11)$  and 0.06 eV for  $(\nu = 1,$

**TABLE 6.5** Minimum barrier height ( $E_b$ , in eV) and energetic corrugation ( $\zeta$ , in eV), of  $\text{H}_2/\text{Cu}(111)$  obtained with the optPBE and PBE exchange functionals combined with PBE correlation.

Exchange functional	$E_b$ (eV)	$\zeta$ (eV)
optPBE	0.460	0.416
PBE	0.484	0.406

$J = 6$ ). The agreement of the static ideal surface theoretical results with the experimental data is not so good for either state and for either functional. However, previous work employing the SRP48 functional<sup>21</sup> and a similar functional (chapter 3) showed that taking into account the effect of the surface temperature used in the experiments ( $925 \text{ K}^{80}$ ) leads to a substantial decrease of the computed  $A_0^{(2)}(\nu, J)$  and to much better agreement with experiment, although the computed  $A_0^{(2)}(\nu, J)$  were still somewhat too high. Taking into account the surface temperature for the optPBE-vdW-DF functional should also lead to a decrease in the  $A_0^{(2)}(\nu, J)$  computed with this functional, and to a better agreement with experiment. It is however not yet clear whether surface temperature has the same quantitative effect for the optPBE-vdW-DF functional, and it is therefore not yet fully clear which functional performs better for  $A_0^{(2)}(\nu, J)$ .

#### 6.3.4 The effect of changing the exchange and the correlation functionals separately

In the above sections, dynamics results for two XC functionals, *i.e.*, the SRP48 and the optPBE-vdW-DF XC functionals, have been discussed. One might wonder whether some of the results that are obtained, such as the better performance of optPBE-vdW-DF for sticking of  $\text{D}_2$  on  $\text{Ru}(0001)$  (figure 6.4) or the difference in performance of the two functionals for reproducing the  $A_0^{(2)}$  measured for  $\text{D}_2/\text{Cu}(111)$  (figure 6.7), is due to changing the exchange functional, the correlation functional, or both. The following can be said about this.

Starting from the SRP48 functional, changing only the exchange functional amounts to using the optPBE exchange functional and the

PBE correlation functional (“optPBE-PBE”). Inspection of table 6.5 suggests that this would yield a functional that is similar to the PBE functional: for  $\text{H}_2/\text{Cu}(111)$ , the minimum barrier height and the energetic corrugation are very similar for these functionals. However, it is known that the PBE functional does not yield a correct description of sticking of  $\text{H}_2$  to  $\text{Ru}(0001)$  (see figure 4.10) because functionals with PBE correlation underestimate the energetic corrugation of the  $\text{H}_2/\text{Ru}(0001)$  PES, as shown in chapter 4. Specifically, with the PBE functional the sticking probability is considerably overestimated at large average collision energies, and the same would be expected to hold for the similar optPBE-PBE functional. In contrast, reasonable values of both the minimum barrier height and the energetic corrugation can be obtained by using vdW-DF correlation. In fact, using SRP48 exchange and vdW-DF correlation would be very similar to using one of the candidate SRP functionals that described sticking of  $\text{H}_2$  and  $\text{D}_2$  to  $\text{Ru}(0001)$  quite well in chapter 4 and even better than the optPBE-vdW-DF functional. Here, the only difference between the SRP48 and the candidate SRP functional is that the former employs 48% RPBE and 52% PBE exchange, whereas the latter uses 50% RPBE and 50% PBE exchange. In other words, the better performance of the optPBE-vdW-DF functional than that of SRP48 comes from changing the PBE to the vdW-DF correlation functional, and not from changing the SRP48 to the optPBE exchange functional.

Similarly, the good performance of the optPBE-vdW-DF functional for  $\text{H}_2/\text{Cu}(111)$  does certainly not come only from changing the SRP48 to the optPBE exchange functional. As discussed above (see again table 6.5) optPBE-PBE and PBE yield very similar values of the minimum barrier height and energetic corrugation of  $\text{H}_2/\text{Cu}(111)$ . However, it is known that using the PW91 functional<sup>6</sup> leads to hugely overestimated sticking probabilities for  $\text{H}_2/\text{Cu}(111)$  when comparing with experimental values.<sup>18</sup> The same should hold for the PBE functional, as the PBE functional was designed to reproduce PW91 energies,<sup>7</sup> and the PBE and PW91 barrier heights for  $\text{H}_2/\text{Cu}(111)$  are indeed very similar.<sup>18</sup> Then, the use of the optPBE-PBE functional should likewise lead to hugely overestimated sticking probabilities for  $\text{H}_2/\text{Cu}(111)$ . Quantum dynamics calculations using a PW91 PES suggest that using the optPBE-

PBE functional to compute  $A_0^{(2)}$  values for  $D_2/\text{Cu}(111)$  should likewise lead to incorrect results: within the static and ideal surface approximation, the use of PW91 leads to computed  $A_0^{(2)}$  values that underestimate the experimental values for ( $\nu = 1, J = 6$ )  $D_2$  (see figure 11 of ref. 59). Also taking into account the effect of the high surface temperature in the experiments ( $925\text{ K}^{80}$ ) would lead to a further decrease of the computed  $A_0^{(2)}$ , as shown in chapter 3 and reference 21, and therefore to an even worse comparison with experiment. In other words, maintaining good agreement with experiment for  $H_2/\text{Cu}(111)$  depends on changing not only the exchange functional, but also the correlation functional when changing the SRP48 XC functional to the optPBE-vdW-DF XC functional.

## 6.4 Conclusions and outlook

Potential energy surfaces are constructed for the dissociation of  $H_2$  on  $\text{Cu}(111)$ ,  $\text{Cu}(100)$ ,  $\text{Pt}(111)$  and  $\text{Ru}(0001)$  from DFT calculations using two different XC functionals, one with non-local vdW-DF correlation (optPBE-vdW-DF) and one with standard GGA (PBE) correlation (SRP48). To determine to what extent using the non-local vdW-DF functional improves the description of the molecule–surface interaction over the non-corrected case, the PESs for the two functionals have been compared to one another in terms of barrier heights, anisotropy in  $\varphi$  and the corrugation in  $U$  and  $V$ . A comparison is also made between reaction probabilities and rotational quadrupole alignment parameters obtained from quasi-classical dynamics calculations and experiments, where possible.

In the analysis of the PESs in terms of barrier heights, different behaviours were found for the weakly activated  $H_2/\text{Pt}(111)$  and  $H_2/\text{Ru}(0001)$  systems on the one hand and the highly activated  $H_2/\text{Cu}(111)$  and  $H_2/\text{Cu}(100)$  systems on the other hand. For  $H_2$  dissociation on  $\text{Ru}(0001)$  and  $\text{Pt}(111)$ , the barriers are generally found to be later for the optPBE-vdW-DF PES than for the SRP48 PES, whereas for  $H_2$  dissociation on  $\text{Cu}(111)$  and  $\text{Cu}(100)$  the barriers were approximately equally late. For  $H_2$  dissociation on  $\text{Ru}(0001)$  and  $\text{Pt}(111)$ , the energetic corrugation (difference in barrier height of the lowest and highest investigated barrier)

is larger for optPBE-*vdW*-DF than for SRP48, whereas for H<sub>2</sub> dissociation on Cu(111) and Cu(100) the opposite is found. This is explained by considering the minimum energy pathways to dissociation for several geometries. For both H<sub>2</sub> dissociation on Ru(0001) and Cu(111), the minimum energy pathways cross at a value of  $Z \approx 1.6 - 1.8 \text{ \AA}$ . If the barrier occurs after this crossing (closer to the surface), as for H<sub>2</sub> dissociation on Cu(111) and Cu(100), the barrier is generally increased because optPBE-*vdW*-DF shows a more steeply rising potential along the reaction path. If the barrier occurs before this crossing, as found for H<sub>2</sub> dissociation on Ru(0001) and Pt(111), the barrier is decreased, because the optPBE-*vdW*-DF functional shows a physisorption well far away from the surface for all considered surfaces, and the barrier is usually also later.

Dynamics results show that reaction probabilities obtained with the optPBE-*vdW*-DF functional tend to be in better overall agreement with experiments than the SRP48 functional. For both D<sub>2</sub> dissociation on Ru(0001) and Pt(111) the optPBE-*vdW*-DF sticking curve is broader (less steep increase with incidence energy) than the SRP48 sticking curve. The primary difference between the sticking curves for the D<sub>2</sub>/Cu(111) and H<sub>2</sub>/Cu(100) systems is a shift, the optPBE-*vdW*-DF functional showing overall less reactivity.

For D<sub>2</sub> dissociating on Cu(111) the  $J$ -dependence of reaction has also been investigated, as well as the vibrational efficacy and the rotational quadrupole alignment parameter. The vibrational efficacy as computed with the optPBE-*vdW*-DF functional is slightly higher than for SRP48. Based on this, and uncertainties in the experimental data, no preference for one of the two tested functionals can be assigned. For the  $J$ -dependence of reaction of D<sub>2</sub> on Cu(111), however, the optPBE-*vdW*-DF functional shows that reaction for low rotational states ( $J < 8$ ) is virtually independent of the rotational state, whereas SRP48 shows reaction to increase with increasing  $J$ . As experimental data for this system shows reaction to decrease with increasing  $J$  state at first, the optPBE-*vdW*-DF results are in qualitatively better agreement with the experimental data. The rotational quadrupole alignment parameter for D<sub>2</sub> on Cu(111) is for both functionals too high compared to experiments. It should be noted however, that the temperature of the surface was not

taken into account in this study. It is known from previous studies that the temperature of the surface can greatly influence the rotational quadrupole alignment parameter. Although the known surface temperature dependence for SRP48 suggests this functional to work better, in order to determine a preference for either functional based on the rotational quadrupole alignment parameter the surface temperature dependence of both functionals should be investigated.

Overall, the optPBE-vdW-DF functional seems to yield results in better agreement with experimental data for the systems considered, especially for the molecular beam sticking probabilities and the width (steepness) of the associated reaction probability curves. It is satisfying to see that including non-local vdW-DF correlation in the XC functional not only improves the description of weakly activated dissociation (as seen for  $\text{H}_2/\text{Ru}(0001)$  in chapter 4), but also of highly activated dissociation.

In the future, it would be of interest to also apply the optPBE-vdW-DF functional to non-activated dissociation problems, such as  $\text{H}_2/\text{Pd}(111)$ ,<sup>81,82</sup>  $\text{H}_2/\text{Pd}(100)$ ,<sup>83,84</sup> or  $\text{H}_2/\text{Ni}(110)$ .<sup>84</sup> A correct description of these systems would demonstrate the correct addition of strongly attractive chemical interactions to the van der Waals interaction in a region that is potentially even closer to the surface, which might constitute an additional challenge. We note that  $\text{H}_2/\text{Pd}(111)$  has already been studied with functionals containing vdW-DF correlation in chapter 5; a problem with this system is that there is considerable uncertainty regarding the experimental sticking probability, due to experimental discrepancies. The  $\text{N}_2/\text{W}(110)$  system, in which the dissociation is also considerably affected by the presence of molecular chemisorption wells, has also recently been studied with the use of vdW functionals.<sup>57</sup> However, the outcome of these calculations should be somewhat uncertain, because the effect of energy transfer to the  $\text{W}(110)$  surface was not yet taken into account, while AIMD calculations suggest a large effect on the reactivity of this energy transfer.<sup>85</sup>

## References

- [1] W. KOHN and L. J. SHAM. Self-consistent equations including exchange and correlation effects. *Physical Review* **140**(4A), A1133–A1138, 1965.

- [2] P. HOHENBERG and W. KOHN. Inhomogeneous electron gas. *Physical Review* **136**(3B), B864–B871, 1964.
- [3] D. C. LANGRETH and M. J. MEHL. Beyond the local-density approximation in calculations of ground-state electronic properties. *Physical Review B* **28**(4), pp. 1809–1834, 1983.
- [4] A. D. BECKE. Density-functional exchange-energy approximation with correct asymptotic behavior. *Physical Review A* **38**(6), pp. 3098–3100, 1988.
- [5] J. P. PERDEW. Density-functional approximation for the correlation energy of the inhomogeneous electron gas. *Physical Review B* **33**(12), pp. 8822–8824, 1986.
- [6] J. P. PERDEW, J. A. CHEVARY, S. H. VOSKO, K. A. JACKSON, M. R. PEDERSON, D. J. SINGH, and C. FIOLEHAIS. Atoms, molecules, solids, and surfaces: applications of the generalized gradient approximation for exchange and correlation. *Physical Review B* **46**(11), pp. 6671–6687, 1992.
- [7] J. P. PERDEW, K. BURKE, and M. ERNZERHOF. Generalized gradient approximation made simple. *Physical Review Letters* **77**(18), pp. 3865–3868, 1996.
- [8] B. HAMMER, L. B. HANSEN, and J. K. NØRSKOV. Improved adsorption energetics within density-functional theory using revised Perdew-Burke-Ernzerhof functionals. *Physical Review B* **59**(11), pp. 7413–7421, 1999.
- [9] J. P. PERDEW and K. SCHMIDT. Jacob’s ladder of density functional approximations for the exchange-correlation energy. *AIP Conference Proceedings* **577**(1), pp. 1–20, 2001.
- [10] J. P. PERDEW, J. TAO, V. N. STAROVEROV, and G. E. SCUSERIA. Meta-generalized gradient approximation: explanation of a realistic nonempirical density functional. *Journal of Chemical Physics* **120**(15), pp. 6898–6911, 2004.
- [11] J. P. PERDEW, A. RUZSINSZKY, G. I. CSONKA, L. A. CONSTANTIN, and J. SUN. Workhorse semilocal density functional for condensed matter physics and quantum chemistry. *Physical Review Letters* **103**(2), 026403, 2009.
- [12] A. D. BECKE. Density-functional thermochemistry. III. The role of exact exchange. *Journal of Chemical Physics* **98**(7), pp. 5648–5652, 1993.
- [13] G. J. KROES. Six-dimensional quantum dynamics of dissociative chemisorption of H<sub>2</sub> on metal surfaces. *Progress in Surface Science* **60**(1–4), pp. 1–85, 1999.
- [14] G. J. KROES and M. F. SOMERS. Six-dimensional dynamics of dissociative chemisorption of H<sub>2</sub> on metal surfaces. *Journal of Theoretical and Computational Chemistry* **04**(02), pp. 493–581, 2005.
- [15] A. GROSS. Reactions at surfaces studied by *ab initio* dynamics calculations. *Surface Science Reports* **32**(8), pp. 291–340, 1998.

- [16] P. NIETO, E. PIJPER, D. BARREDO, G. LAURENT, R. A. OLSEN, E. J. BAERENDS, G. J. KROES, and D. FARIAS. Reactive and nonreactive scattering of  $H_2$  from a metal surface is electronically adiabatic. *Science* **312**(5770), pp. 86–89, 2006.
- [17] M. POZZO and D. ALFÈ. Hydrogen dissociation on Mg(0001) studied via quantum Monte Carlo calculations. *Physical Review B* **78**(24), 245313, 2008.
- [18] C. DÍAZ, E. PIJPER, R. A. OLSEN, H. F. BUSNENGO, D. J. AUERBACH, and G. J. KROES. Chemically accurate simulation of a prototypical surface reaction:  $H_2$  dissociation on Cu(111). *Science* **326**(5954), pp. 832–834, 2009.
- [19] A. GROSS. *Ab initio* molecular dynamics simulations of the adsorption of  $H_2$  on palladium surfaces. *ChemPhysChem* **11**(7), pp. 1374–1381, 2010.
- [20] P. NIETO, D. FARIAS, R. MIRANDA, M. LUPPI, E. J. BAERENDS, M. F. SOMERS, M. J. T. C. VAN DER NIET, R. A. OLSEN, and G. J. KROES. Diffractive and reactive scattering of  $H_2$  from Ru(0001): experimental and theoretical study. *Physical Chemistry Chemical Physics* **13**(18), pp. 8583–8597, 2011.
- [21] F. NATTINO, C. DÍAZ, B. JACKSON, and G. J. KROES. Effect of surface motion on the rotational quadrupole alignment parameter of  $D_2$  reacting on Cu(111). *Physical Review Letters* **108**(23), 236104, 2012.
- [22] G. FÜCHSEL, S. SCHIMKA, and P. SAALFRANK. On the role of electronic friction for dissociative adsorption and scattering of hydrogen molecules at a Ru(0001) surface. *Journal of Physical Chemistry A* **117**(36), pp. 8761–8769, 2013.
- [23] G. J. KROES and C. DÍAZ. Quantum and classical dynamics of reactive scattering of  $H_2$  from metal surfaces. Accepted to *Chemical Society Reviews*. doi: 10.1039/C5CS00336A. 2016.
- [24] G. J. KROES. Frontiers in surface scattering simulations. *Science* **321**(5890), pp. 794–797, 2008.
- [25] G. J. KROES. Towards chemically accurate simulation of molecule-surface reactions. *Physical Chemistry Chemical Physics* **14**(43), pp. 14966–14981, 2012.
- [26] A. C. LUNTZ and M. PERSSON. How adiabatic is activated adsorption/associative desorption? *Journal of Chemical Physics* **123**(7), 074704, 2005.
- [27] A. S. MUZAS, J. I. JUARISTI, M. ALDUCIN, R. DÍEZ MUIÑO, G. J. KROES, and C. DÍAZ. Vibrational deexcitation and rotational excitation of  $H_2$  and  $D_2$  scattered from Cu(111): adiabatic versus non-adiabatic dynamics. *Journal of Chemical Physics* **137**(6), 064707, 2012.
- [28] J. I. JUARISTI, M. ALDUCIN, R. DÍEZ MUIÑO, H. F. BUSNENGO, and A. SALIN. Role of electron-hole pair excitations in the dissociative adsorption of diatomic molecules on metal surfaces. *Physical Review Letters* **100**(11), 116102, 2008.

- [29] H. F. BUSNENGO, W. DONG, P. SAUTET, and A. SALIN. Surface temperature dependence of rotational excitation of  $H_2$  scattered from Pd(111). *Physical Review Letters* **87**(12), 127601, 2001.
- [30] H. F. BUSNENGO, M. A. DI CÉSARE, W. DONG, and A. SALIN. Surface temperature effects in dynamic trapping mediated adsorption of light molecules on metal surfaces:  $H_2$  on Pd(111) and Pd(110). *Physical Review B* **72**(12), 125411, 2005.
- [31] H. F. BUSNENGO, A. SALIN, and W. DONG. Representation of the 6D potential energy surface for a diatomic molecule near a solid surface. *Journal of Chemical Physics* **112**(17), pp. 7641–7651, 2000.
- [32] R. A. OLSEN, H. F. BUSNENGO, A. SALIN, M. F. SOMERS, G. J. KROES, and E. J. BAERENDS. Constructing accurate potential energy surfaces for a diatomic molecule interacting with a solid surface:  $H_2+Pt(111)$  and  $H_2+Cu(100)$ . *Journal of Chemical Physics* **116**(9), pp. 3841–3855, 2002.
- [33] M. DION, H. RYDBERG, E. SCHRÖDER, D. C. LANGRETH, and B. I. LUNDQVIST. Van der Waals density functional for general geometries. *Physical Review Letters* **92**(24), 246401, 2004.
- [34] K. LEE, E. D. MURRAY, L. KONG, B. I. LUNDQVIST, and D. C. LANGRETH. Higher-accuracy van der Waals density functional. *Physical Review B* **82**(8), 081101, 2010.
- [35] J. ZHENG, Y. ZHAO, and D. G. TRUHLAR. The DBH24/08 database and its use to assess electronic structure model chemistries for chemical reaction barrier heights. *Journal of Chemical Theory and Computation* **5**(4), pp. 808–821, 2009.
- [36] K. YANG, J. ZHENG, Y. ZHAO, and D. G. TRUHLAR. Tests of the RPBE, revPBE,  $\tau$ -HCTHhyb,  $\omega$ B97X-D, and MOHLYP density functional approximations and 29 others against representative databases for diverse bond energies and barrier heights in catalysis. *Journal of Chemical Physics* **132**(16), 164117, 2010.
- [37] R. PEVERATI and D. G. TRUHLAR. Quest for a universal density functional: the accuracy of density functionals across a broad spectrum of databases in chemistry and physics. *Philosophical Transactions of the Royal Society of London A* **372**(2011), 20120476, 2014.
- [38] R. PEVERATI and D. G. TRUHLAR. M11-L: A local density functional that provides improved accuracy for electronic structure calculations in chemistry and physics. *Journal of Physical Chemistry Letters* **3**(1), pp. 117–124, 2012.
- [39] R. PEVERATI and D. G. TRUHLAR. An improved and broadly accurate local approximation to the exchange-correlation density functional: the MN12-L functional for electronic structure calculations in chemistry and physics. *Physical Chemistry Chemical Physics* **14**(38), pp. 13171–13174, 2012.

- [40] H. S. YU, X. HE, and D. G. TRUHLAR. MN15-L: a new local exchange–correlation functional for Kohn–Sham density functional theory with broad accuracy for atoms, molecules, and solids. *Journal of Chemical Theory and Computation* **12**(3), pp. 1280–1293, 2016.
- [41] Y. Y. CHUANG, M. L. RADHAKRISHNAN, P. L. FAST, C. J. CRAMER, and D. G. TRUHLAR. Direct dynamics for free radical kinetics in solution: solvent effect on the rate constant for the reaction of methanol with atomic hydrogen. *Journal of Physical Chemistry A* **103**(25), pp. 4893–4909, 1999.
- [42] L. SEMENTA, M. WIJZENBROEK, B. J. VAN KOLCK, M. F. SOMERS, A. AL-HALABI, H. F. BUSNENGO, R. A. OLSEN, G. J. KROES, M. RUTKOWSKI, C. THEWES, N. F. KLEIMEIER, and H. ZACHARIAS. Reactive scattering of H<sub>2</sub> from Cu(100): comparison of dynamics calculations based on the specific reaction parameter approach to density functional theory with experiment. *Journal of Chemical Physics* **138**(4), 044708, 2013.
- [43] A. TKATCHENKO, L. ROMANER, O. T. HOFMANN, E. ZOJER, C. AMBROSCH-DRAXL, and M. SCHEFFLER. Van der Waals interactions between organic adsorbates and at organic/inorganic interfaces. *MRS Bulletin* **35**(6), pp. 435–442, 2010.
- [44] S. GRIMME. Density functional theory with London dispersion corrections. *Wiley Interdisciplinary Reviews: Computational Molecular Science* **1**(2), pp. 211–228, 2011.
- [45] J. KLIMEŠ and A. MICHAELIDES. Perspective: Advances and challenges in treating van der Waals dispersion forces in density functional theory. *Journal of Chemical Physics* **137**(12), 120901, 2012.
- [46] J. P. P. RAMALHO, J. R. B. GOMES, and F. ILLAS. Accounting for van der Waals interactions between adsorbates and surfaces in density functional theory based calculations: selected examples. *RSC Advances* **3**(32), pp. 13085–13100, 2013.
- [47] K. BERLAND, V. R. COOPER, K. LEE, E. SCHRÖDER, T. THONHAUSER, P. HYLDGAARD, and B. I. LUNDQVIST. van der Waals forces in density functional theory: a review of the vdW-DF method. *Reports on Progress in Physics* **78**(6), 066501, 2015.
- [48] S. GRIMME, J. ANTONY, S. EHRLICH, and H. KRIEG. A consistent and accurate *ab initio* parameterization of density functional dispersion correction (DFT-D) for the 94 elements H–Pu. *Journal of Chemical Physics* **132**(15), 154104, 2010.
- [49] A. TKATCHENKO and M. SCHEFFLER. Accurate molecular van der Waals interactions from ground-state electron density and free-atom reference data. *Physical Review Letters* **102**(7), 073005, 2009.
- [50] J. KLIMEŠ, D. R. BOWLER, and A. MICHAELIDES. Chemical accuracy for the van der Waals density functional. *Journal of Physics: Condensed Matter* **22**(2), 022201, 2010.

- [51] J. KLIMEŠ, D. R. BOWLER, and A. MICHAELIDES. Van der Waals density functionals applied to solids. *Physical Review B* **83**(19), 195131, 2011.
- [52] V. R. COOPER. Van der Waals density functional: An appropriate exchange functional. *Physical Review B* **81**(16), 161104(R), 2010.
- [53] K. BERLAND and P. HYLDGAARD. Exchange functional that tests the robustness of the plasmon description of the van der Waals density functional. *Physical Review B* **89**(3), 035412, 2014.
- [54] W. LIU, J. CARRASCO, B. SANTRA, A. MICHAELIDES, M. SCHEFFLER, and A. TKATCHENKO. Benzene adsorbed on metals: concerted effect of covalency and van der Waals bonding. *Physical Review B* **86**(24), 245405, 2012.
- [55] H. YILDIRIM, T. GREBER, and A. KARA. Trends in adsorption characteristics of benzene on transition metal surfaces: role of surface chemistry and van der Waals interactions. *Journal of Physical Chemistry C* **117**(40), pp. 20572–20583, 2013.
- [56] J. CARRASCO, W. LIU, A. MICHAELIDES, and A. TKATCHENKO. Insight into the description of van der Waals forces for benzene adsorption on transition metal (111) surfaces. *Journal of Chemical Physics* **140**(8), 084704, 2014.
- [57] L. MARTIN-GONDRE, J. I. JUARISTI, M. BLANCO-REY, R. DÍEZ MUIÑO, and M. ALDUCIN. Influence of the van der Waals interaction in the dissociation dynamics of  $N_2$  on W(110) from first principles. *Journal of Chemical Physics* **142**(7), 074704, 2015.
- [58] M. BORN and R. OPPENHEIMER. Zur Quantentheorie der Molekeln. *Annalen der Physik* **389**(20), pp. 457–484, 1927.
- [59] C. DÍAZ, R. A. OLSEN, D. J. AUERBACH, and G. J. KROES. Six-dimensional dynamics study of reactive and non reactive scattering of  $H_2$  from Cu(111) using a chemically accurate potential energy surface. *Physical Chemistry Chemical Physics* **12**(24), pp. 6499–6519, 2010.
- [60] A. MONDAL, M. WIJZENBROEK, M. BONFANTI, C. DÍAZ, and G. J. KROES. Thermal lattice expansion effect on reactive scattering of  $H_2$  from Cu(111) at  $T_s = 925$  K. *Journal of Physical Chemistry A* **117**(36), pp. 8770–8781, 2013.
- [61] D. A. McCORMACK and G. J. KROES. Accuracy of trajectory methods for activated adsorption of  $H_2$  on Cu(100). *Chemical Physics Letters* **296**(5–6), pp. 515–520, 1998.
- [62] E. PIJPER, M. F. SOMERS, G. J. KROES, R. A. OLSEN, E. J. BAERENDS, H. F. BUSNENGO, A. SALIN, and D. LEMOINE. Six-dimensional quantum dynamics of scattering of ( $v=0, j=0$ )  $H_2$  from Pt(111): comparison to experiment and to classical dynamics results. *Chemical Physics Letters* **347**(4–6), pp. 277–284, 2001.

- [63] J. STOER and R. BULIRSCH. *Introduction to numerical analysis*. New York: Springer, 1980.
- [64] G. KRESSE and J. HAFNER. *Ab initio* molecular dynamics for liquid metals. *Physical Review B* **47**(1), pp. 558–561, 1993.
- [65] G. KRESSE and J. FURTHMÜLLER. Efficiency of *ab initio* total energy calculations for metals and semiconductors using a plane-wave basis set. *Computational Materials Science* **6**(1), pp. 15–50, 1996.
- [66] G. KRESSE and J. FURTHMÜLLER. Efficient iterative schemes for *ab initio* total-energy calculations using a plane-wave basis set. *Physical Review B* **54**(16), pp. 11169–11186, 1996.
- [67] G. KRESSE and D. JOUBERT. From ultrasoft pseudopotentials to the projector augmented-wave method. *Physical Review B* **59**(3), pp. 1758–1775, 1999.
- [68] G. KRESSE and J. HAFNER. Norm-conserving and ultrasoft pseudopotentials for first-row and transition elements. *Journal of Physics: Condensed Matter* **6**(40), pp. 8245–8257, 1994.
- [69] D. VANDERBILT. Soft self-consistent pseudopotentials in a generalized eigenvalue formalism. *Physical Review B* **41**(11), pp. 7892–7895, 1990.
- [70] P. E. BLÖCHL. Projector augmented-wave method. *Physical Review B* **50**(24), pp. 17953–17979, 1994.
- [71] G. ROMÁN-PÉREZ and J. M. SOLER. Efficient implementation of a van der Waals density functional: application to double-wall carbon nanotubes. *Physical Review Letters* **103**(9), 096102, 2009.
- [72] M. LUPPI, R. A. OLSEN, and E. J. BAERENDS. Six-dimensional potential energy surface for H<sub>2</sub> at Ru(0001). *Physical Chemistry Chemical Physics* **8**(6), pp. 688–696, 2006.
- [73] H. A. MICHELSEN, C. T. RETTNER, D. J. AUERBACH, and R. N. ZARE. Effect of rotation on the translational and vibrational energy dependence of the dissociative adsorption of D<sub>2</sub> on Cu(111). *Journal of Chemical Physics* **98**(10), pp. 8294–8307, 1993.
- [74] G. ANGER, A. WINKLER, and K. D. RENDULIC. Adsorption and desorption kinetics in the systems H<sub>2</sub>/Cu(111), H<sub>2</sub>/Cu(110) and H<sub>2</sub>/Cu(100). *Surface Science* **220**(1), pp. 1–17, 1989.
- [75] A. C. LUNTZ, J. K. BROWN, and M. D. WILLIAMS. Molecular beam studies of H<sub>2</sub> and D<sub>2</sub> dissociative chemisorption on Pt(111). *Journal of Chemical Physics* **93**(7), pp. 5240–5246, 1990.

- [76] I. M. N. GROOT, H. UETA, M. J. T. C. VAN DER NIET, A. W. KLEYN, and L. B. F. JUURLINK. Supersonic molecular beam studies of dissociative adsorption of  $H_2$  on Ru(0001). *Journal of Chemical Physics* **127**(24), 244701, 2007.
- [77] F. NATTINO, A. GENOVA, M. GUIJT, A. S. MUZAS, C. DÍAZ, D. J. AUERBACH, and G. J. KROES. Dissociation and recombination of  $D_2$  on Cu(111): *ab initio* molecular dynamics calculations and improved analysis of desorption experiments. *Journal of Chemical Physics* **141**(12), 124705, 2014.
- [78] H. A. MICHELSEN, C. T. RETTNER, and D. J. AUERBACH. On the influence of surface temperature on adsorption and desorption in the  $D_2$ /Cu(111) system. *Surface Science* **272**(1–3), pp. 65–72, 1992.
- [79] M. J. MURPHY and A. HODGSON. Adsorption and desorption dynamics of  $H_2$  and  $D_2$  on Cu(111): the role of surface temperature and evidence for corrugation of the dissociation barrier. *Journal of Chemical Physics* **108**(10), pp. 4199–4211, 1998.
- [80] H. HOU, S. J. GULDING, C. T. RETTNER, A. M. WODTKE, and D. J. AUERBACH. The stereodynamics of a gas-surface reaction. *Science* **277**(5322), pp. 80–82, 1997.
- [81] J. LESNIK. Untersuchungen über Vorläuferadsorption an Übergangsmetallen und Übergangsmetallegierungen. PhD thesis. Technischen Universität Graz, 2001.
- [82] M. BEUTL, J. LESNIK, K. D. RENDULIC, R. HIRSCHL, A. EICHLER, G. KRESSE, and J. HAFNER. There is a true precursor for hydrogen adsorption after all: the system  $H_2$ /Pd(111) + subsurface V. *Chemical Physics Letters* **342**(5–6), pp. 473–478, 2001.
- [83] C. T. RETTNER and D. J. AUERBACH. Search for oscillations in the translational energy dependence of the dissociation of  $H_2$  on Pd(100). *Chemical Physics Letters* **253**(3–4), pp. 236–240, 1996.
- [84] K. D. RENDULIC, G. ANGER, and A. WINKLER. Wide range nozzle beam adsorption data for the systems  $H_2$ /nickel and  $H_2$ /Pd(100). *Surface Science* **208**(3), pp. 404–424, 1989.
- [85] F. NATTINO, F. COSTANZO, and G. J. KROES.  $N_2$  dissociation on W(110): an *ab initio* molecular dynamics study on the effect of phonons. *Journal of Chemical Physics* **142**(10), 104702, 2015.